

NEW STUDIES OF THE PULSAR WIND NEBULA IN THE SUPERNOVA REMNANT CTB 80

T. A. Lozinskaya^{1*}, V. N. Komarova², A. V. Moiseev², S. I. Blinnikov²

¹ Sternberg Astronomical Institute, Universitetskii pr. 13, Moscow, 119992 Russia

² Special Astrophysical Observatory, Russian Academy of Sciences, Nizhnii Arkhyz, Karachai-Cherkessian Republic, 357147 Russia

³ Institute for Theoretical and Experimental Physics, ul. Bol'shaya Cheredushkinskaya 25, Moscow, 117259 Russia

Received — November 15, 2004

Abstract. We investigated the kinematics of the pulsar wind nebula (PWN) associated with PSR B1951+32 in the old supernova remnant CTB 80 using the Fabry–Perot interferometer of the 6 m Special Astrophysical Observatory telescope. In addition to the previously known expansion of the system of bright filaments with a velocity of 100–200 km s⁻¹, we detected weak high-velocity features in the H α line at least up to velocities of 400–450 km s⁻¹. We analyzed the morphology of the PWN in the H α , [SII], and [OIII] lines using HST archival data and discuss its nature. The shape of the central filamentary shell, which is determined by the emission in the [OIII] line and in the radio continuum, is shown to be consistent with the bow-shock model for a significant (about 60°) inclination of the pulsar's velocity vector to the plane of the sky. In this case, the space velocity of the pulsar is twice higher than its tangential velocity, i.e., it reaches $\simeq 500$ km s⁻¹, and PSR B1951+32 is the first pulsar whose line-of-sight velocity (of about 400 km/s) has been estimated from the PWN observations. The shell-like H α -structures outside the bow shock front in the east and the west may be associated with both the pulsar's jets and the pulsar-wind breakthrough due to the layered structure of the extended CTB 80 shell.

Key words. Supernovae and supernova remnants, pulsar wind nebulae, models.

INTRODUCTION

CTB 80 is a classical example of a supernova remnant (SNR) with a fast-moving pulsar at a late stage of the pulsar's interaction with a very old shell.

The radio image of CTB 80 is represented by three extended (about 30') ridges that converge in the region of a bright compact core (Velusami and Kundu 1974; Velusami *et al.* 1976; Angerhofer *et al.* 1981; Strom *et al.* 1984; Mantovani *et al.* 1985; Strom 1987; Castelletti *et al.* 2003, and references therein). This unusual (for SNRs) morphology ceased to appear puzzling in 1988, when, on the one hand, the 39.5-ms pulsar PSR B1951+32 was discovered in the core (Kulkarni *et al.* 1988; Fruchter *et al.* 1988) and, on the other hand, Fesen *et al.* (1988) identified an extended infrared shell that extends the radio ridges in the northeast and assumed that precisely this infrared shell represents a very old SNR. The radio ridges with a steep spectrum ($\alpha \simeq -0.7$) correspond to the part of the shell into the compressed magnetic field of which the approached pulsar injected fresh relativistic particles, thereby reanimating its synchrotron radio emission. Subsequently, an HI

shell that coincides with the infrared shell and expands with a velocity of 72 km s⁻¹, which yields a kinematic SNR age of 7.7×10^4 yr, was also identified (Koo *et al.* 1990, 1993). The characteristic age of the pulsar PSR B1951+32 is $t \simeq 10^5$ yr (Kulkarni *et al.* 1988; Fruchter *et al.* 1988).

The pulsar wind nebula (PWN) is represented by a bright compact (45'') core with a flat spectrum ($\alpha \simeq 0.0$). The core lies at the western boundary of a 10' \times 6' plateau with a steeper spectrum ($\alpha \simeq -0.3$) elongated in the east–west direction. Recently, Migliazzo *et al.* (2002) detected the motion of the pulsar with a velocity of 240 km s⁻¹ in a direction that confirms the possibility of its birth inside the infrared and HI shells.

The stage of pulsar wind interaction with a very old shell observed in CTB 80 seems most complex in the evolutionary chain of PWNs, from young SNRs where the pulsar interacts with the SN ejection to pulsars that have already escaped from the old SNR. The difficulty lies in the fact that the matter density in the cooled old shell behind the front of the decelerated shock (and, hence, the density of the compressed interstellar magnetic field) is several hundred times higher than the ambient density and the shell structure is unpredictable in advance. In addition,

*E-mail: lozinsk@sai.msu.ru

the rotational energy loss by the pulsar PSR B1951+32 is large ($\dot{E} = 3.7 \times 10^{36}$ erg s⁻¹, as estimated by Kulkarni *et al.* 1988), which is comparable to the energy input from the young Vela X pulsar.

Various distance estimates for CTB 80 and the pulsar PSR B1951+32 lie within the range 1.5–2.5 kpc (see Koo *et al.* 1993; Strom and Stappers 2000; and references therein); we use the universally accepted distance of 2 kpc.

In this paper, we present our observations of the PWN in CTB 80 with the 6 m Special Astrophysical Observatory (SAO) telescope and analyze narrow-band observational data from the HST archive.

OBSERVATIONS AND DATA REDUCTION

Interferometric Observations on the 6 m Telescope

The core of CTB 80 was observed with the 6 m telescope as part of a program entitled “The Kinematics of Matter in Pulsar Wind Nebulae” (the main applicant is Yu.A. Shibano). Our interferometric observations of CTB 80 were performed on October 9–10, 2001, at the prime focus of the 6 m telescope using the SCORPIO focal reducer; the equivalent focal ratio of the system was $F/2.9$. A description of SCORPIO is given in the paper by Afanasiev and Moiseev (2005) and on the Internet (<http://www.sao.ru/hq/moisav/scorpio/scorpio.html>); the SCORPIO capabilities in interferometric observations were described by Moiseev (2002). The seeing during the observations varied within the range 1''2–2''2. We used a scanning Fabry–Perot interferometer (FPI) in the 235th order at the wavelength of the H α line; the separation between the neighboring orders of interference, $\Delta\lambda = 28$ Å, corresponded to a region free from order overlapping of 1270 km s⁻¹ on the radial velocity scale. The width of the instrumental FPI profile was $FWHM \approx 2.5$ Å or ≈ 110 –120 km s⁻¹. Premonochromatization was performed using an interference filter with a half-width of $\Delta\lambda = 14$ Å centered on the H α line. The detector was a TK1024 1024 × 1024-pixel CCD array. The observations were carried out with 2 × 2-pixel binning to reduce the readout time. In each spectral channel, we obtained 512 × 512-pixel images; at a 0.55''/pixel scale, the total field of view was 4'.7. We obtained a total of 32 interferograms at various FPI plate spacings, so the width of the spectral channel was $\delta\lambda = 0.87$ Å or 40 km s⁻¹ near H α . The exposure time was 240 s per channel.

We reduced the observations using software running in the IDL environment (Moiseev 2002). After the primary reduction (debiasing and flat fielding), the observational data were represented as 512 × 512 × 32-pixel data cubes; here, a 32-channel spectrum corresponds to each pixel. Major difficulties in the data reduction process arose when night-sky emission lines were subtracted from interferograms. All bright image features were masked, and an azimuthally averaged radial sky emission line profile was constructed from the remaining areas; this profile was subtracted from the corresponding frame in the data

cube. This technique allows the sky line intensity variations during two-hour observations to be effectively corrected. However, almost the entire field of view near the core of CTB 80 proved to be filled with weak emission features, which was also confirmed by our deep H α images of the PWN. Therefore, the problem of choosing a sufficient number of “clean” sky areas in a region of almost 5' in size arose. As a result, the weakest features in the field of view could be “oversubtracted”, and the H α emission line profile is severely distorted at these locations. Our estimates indicate that the line distortion due to the background subtraction may be disregarded for regions in which the intensity of the H α line exceeds 150 photoelectrons per CCD pixel, which corresponds to a surface brightness of 8.6×10^{-17} erg s⁻¹/□'' (uncorrected for the interstellar reddening).

The large number of background stars in the field allowed us to measure and correct the atmospheric transparency and seeing variations in each image. The resulting seeing was 2''2. Subsequently, we reduced the spectra in the data cube to the same wavelength scale. The formal accuracy of measuring the relative line-of-sight velocities was about 2–4 km s⁻¹. However, since the emission lines in the object often have asymmetric profiles, the actual measurement accuracy depends on the chosen line profile fitting method.

The spectra of the object were smoothed with a $FWHM = 1.7$ Å (two channels) Gaussian for optimal filtering of the data cube. To reliably identify weak emission features, we also smoothed the images in the cube with a bivariate Gaussian. The resultant angular resolution was about 2''6. The smoothing was performed using the ADHOC software package¹.

The continuum level in each spectrum was determined as a median mean of the eight weakest levels. When constructing the velocity field and the monochromatic image in the H α line, we fitted the spectral line profile by a Gaussian using only the points offset by ± 3 channels from the predetermined line peak.

We calibrated the monochromatic image in energy units (erg s⁻¹ cm⁻²) by comparison with our calibrated narrow-band image (see below).

All of the radial velocities in this paper are heliocentric; the passage to the Local Standard of Rest corresponds to $V_{\text{Hel}} = V_{\text{LSR}} + 17.6$ km s⁻¹.

Medium- and Narrow-Band Images

Observations with the 6 m telescope. Our medium- and narrow-band observations of the CTB 80 core were performed on October 11 and 12, 2001, with the 6 m telescope using the SCORPIO focal reducer (see above) at seeing 1''4–1''6 at zenith distance $z = 12^\circ$ – 21° . Filter parameters and exposure times are given in the Table.

¹ The ADHOC software package was developed by J. Boulestex (Marseilles Observatory) and is freely accessible on the Internet.

Details of the narrow- and medium-band observations of the CTB 80 core with the 6 m telescope (BTA) and HST

Range, telescope	Filter	$\lambda_{\text{cen}}, \text{\AA}$	$FWHM, \text{\AA}$	Exposure time, s
H α , BTA	FN657	6578	75	4 \times 300
Continuum, BTA	SED707	7036	207	4 \times 120
H α , HST	F656N	6563	20	2600 + 2700
Continuum, HST	F547M	5479	200	1300 + 1300
[OIII], HST	F502N	5013	20	2700 + 2700
[SII], HST	F673N	6732	20	2700 + 2700

To calibrate the images, we observed the spectrophotometric standards G138–31 and Feige 110.

The HST archive. The PWN in CTB 80 was observed with HST (the main applicant is J. Trauger) in October 1997 using the WFPC2 instrument. Parameters of the filters used and the total exposure time are given in the Table. The primary data reduction is automatically performed when the data are queried from the HST archive. A filtering code proposed by N.A. Tikhonov (private communication) was used to remove numerous cosmic-ray particle hits. The formal accuracy of the astrometric referencing using WCSTools is an order of magnitude lower than the internal accuracy of the USNO-A2.0 star catalog used as a reference one. The resultant value was taken to be 0".3.

RESULTS OF OBSERVATIONS

The PWN Morphology

Previous studies of the CTB 80 core showed that its optical emission is typical of SNRs: an intense (relative to H α) [NII], [SII], [OI], [OIII] line emission and a filamentary structure (see Angerhofer *et al.* 1980; Blair *et al.* 1984; Whitehead *et al.* 1989; Hester and Kulkarni 1988, 1989; and references therein). Significant differences in the PWN morphology in different lines were reported: only a symmetric central shell is observed in the [OIII] line, a shell to the east of it appears in the [SII] line, and two bright shells to the east and the west of the central structure that form an elongated core structure are observed in the H α line.

The deep HST images of the PWN demonstrate a staggering filamentary, irregularly shaped multishell structure and confirm the results of ground-based observations (see Fig. 1, which shows the [OIII], [SII], and H α images, from top to bottom panels, respectively, with superimposed VLA 1.5-GHz radio isophotes).

Only the central horseshoe-shaped part of the core closest to the pulsar is seen in the [OIII] line. The PWN morphology in the [OIII] line clearly shows a structure expected for the bow shock produced by the pulsar's motion (see the discussion). The H α emission is also observed in this central filamentary horseshoe-shaped shell; the H α filaments are adjacent to the [OIII] filaments from

the outside. We clearly see the two bright (in H α) filamentary shells in the east and the west, which form a spindle-shaped core structure in the east–west direction. The PWN sizes in the H α line are about 75" \times 38" or 0.73 \times 0.37 pc.

The PWN Kinematics

The velocities of PWN filaments. The comparisons of relative line intensities in the core spectrum with diagnostic models made by several authors are suggestive of collisional excitation of the gas behind the front of a shock propagating at a velocity of about 120–140 km s $^{-1}$ in a medium with a density of 25–100 cm $^{-3}$ (Hester and Kulkarni 1989, and references therein). Gas motions in the PWN with such velocities have already been detected. The main method used was long-slit spectroscopy, which allowed the velocities of the individual, generally brightest (and, hence, possibly slowest) knots and filaments to be estimated (Angerhofer *et al.* 1981; Blair *et al.* 1984). Spectroscopic methods did not reveal radial velocities higher than 200 km s $^{-1}$ with a surface brightness at H α \geq 0.5 10 $^{-6}$ erg cm $^{-2}$ s $^{-1}$ sr $^{-1}$ anywhere in the PWN (Blair *et al.* 1988). Using the echelle spectrograph of the 4-m WHT telescope, Whitehead *et al.* (1989) found an expansion of the two central shells with velocities of 200 and 100 km s $^{-1}$.

Using FPI, we have studied the PWN kinematics for the first time. The advantage of FPI observations is that they give the line profile everywhere in the PWN, and not only in the region cut out by the spectrograph slit.

Our observations indicate that the line profile, which is single in bright peripheral filaments, is characterized by a multicomponent structure or line asymmetry, bright red wings in the central PWN regions. As an illustration, several profiles and their decomposition into individual Gaussians are given in Fig. 2. Having analyzed all of the observed H α profiles, we were able to localize the high-velocity gas in the PWN image that emits in the range from 200 to 400 km s $^{-1}$ (shown at the center in Fig. 2).

Figure 3 shows several so-called position–velocity diagrams (the change in gas velocity along the chosen direction) constructed from our FPI observations and the localization of the corresponding directions in the PWN image.

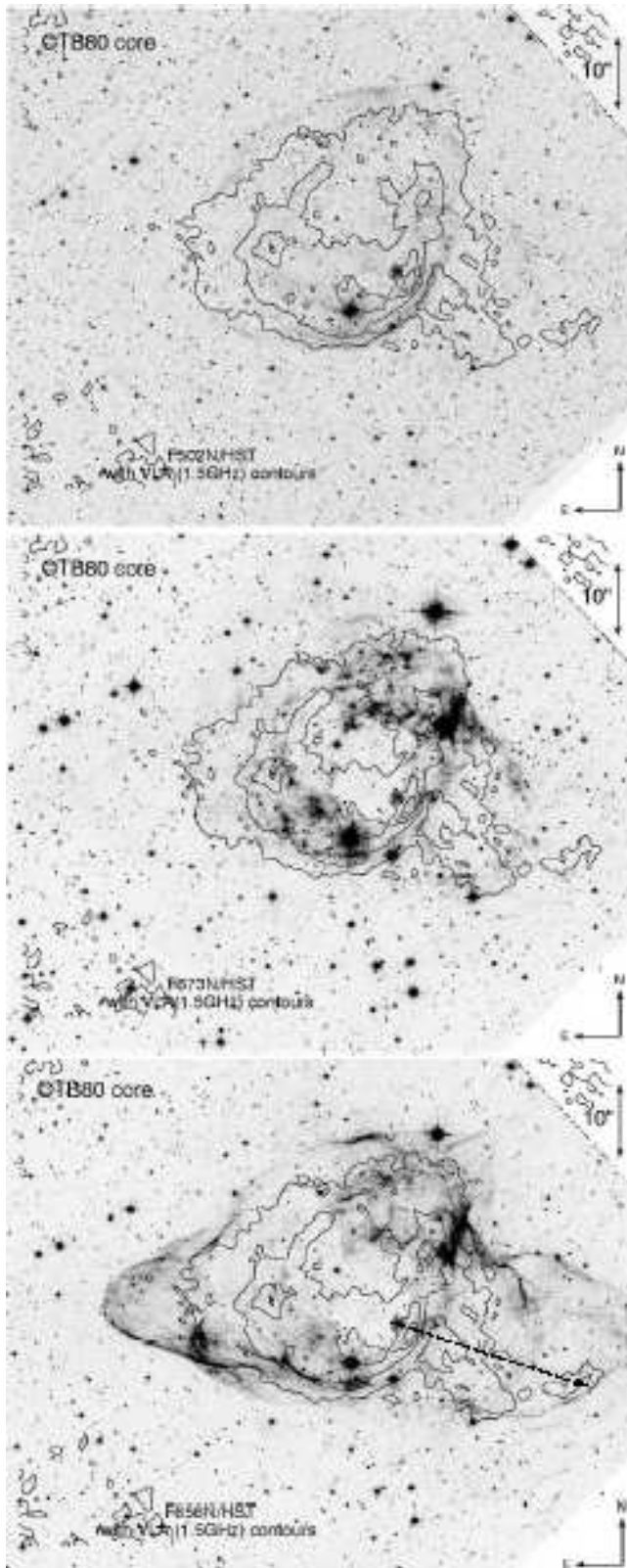


Fig. 1. HST images of the PWN with superimposed VLA 1.5-GHz radio isophotes: in the [OIII] line (*top*), in the [SII] line (*middle*), and in the $H\alpha$ line (*bottom panel*). The arrow indicates the motion of the pulsar over a period of 1000 yr, as measured by Migliazzo *et al.* (2002).

As we see from this figure, in the bright core structures, the position–velocity diagrams show velocities that agree with the previously measured expansion velocity of 100–200 km s^{−1}; i.e., they completely confirm the results of spectroscopic observations.

In addition to the gas velocities in bright filaments within the range from −200 to +200 km s^{−1}, our observations clearly reveal weaker high-velocity $H\alpha$ emission features in the PWN. Weak emission at high velocities is clearly seen in the position–velocity diagrams up to 400–450 km s^{−1}. This is a lower limit, since the velocity range is limited by the FPI velocity range free from order overlapping and the impossibility to properly take into account the contribution from the [NII] 6548 Å line emission.

Figure 3 (scan 3) clearly shows the typical (for an expanding shell) structure of the so-called velocity ellipsoid (its half corresponding to positive velocities) that is determined by high-velocity motions. The corresponding possible expansion velocity reaches the lower limit mentioned above.

The surface brightness of the detected high-velocity component of the $H\alpha$ line in the central part of the core lies within the range $(1.4\text{--}20) \times 10^{-16}$ erg s^{−1} cm^{−2} arcsec^{−2}. In our estimation, we took the color excess $E(B-V) = 0.8$ from Blair *et al.* (1984).

Figure 4 shows the line-of-sight velocity field corresponding to the peak of the main line component constructed from our observations and superimposed on the $H\alpha$ image of the PWN. We emphasize that the line-of-sight velocity field refers only to the core of the line, which often has a complex multicomponent profile. The velocities determined from the line peak lie within the range −100 to +50 km s^{−1}, in agreement with the spectroscopic observations.

In Fig. 4, we clearly see the symmetry axis in the velocity distribution of the peak of the main line component in a direction $P \approx 230^\circ$, which is close to but does not coincide with the direction of the pulsar’s motion ($P = 252^\circ \pm 7^\circ$; Migliazzo *et al.* 2002).

We estimated the total flux from the PWN in the main line component to be 8.4×10^{-12} erg s^{−1} cm^{−2}, in close agreement with the estimate of Whitehead *et al.* (1989). The total flux in the high-velocity line component is 6.4×10^{-13} erg s^{−1} cm^{−2}; the luminosity of the high-velocity gas accounts for about 7% of the total luminosity of the core in the $H\alpha$ line.

The high-velocity emission detected in the core for the first time has confirmed the changes in the PWN fine structure pointed out by Strom and Blair (1985) — possibly the proper motions of the filaments of the central shell corresponding to a velocity of $250d$ km s^{−1} (up to $400d$ km s^{−1}), where d is the distance to CTB 80 in kpc, i.e., about 500 km s^{−1} (possibly up to 800 km s^{−1}).

The velocities of filaments in the CTB 80 shell outside the core. The optical radiation from the extended SNR CTB 80 outside the PWN is represented by the system of faint filaments clearly seen in the [SII] and

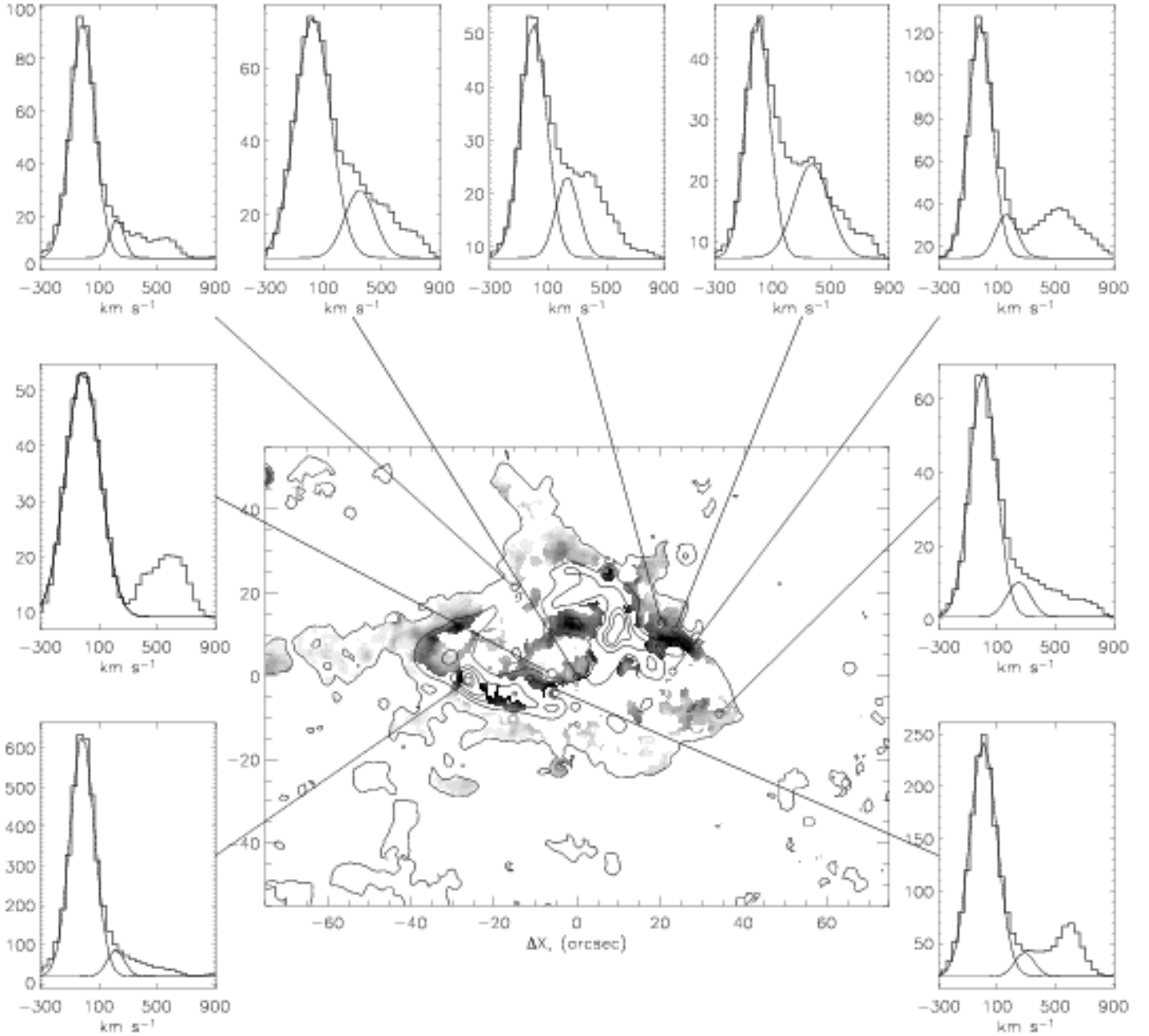


Fig. 2. $H\alpha$ profiles at several points of the PWN and their Gaussian decomposition. The features at a velocity of $+605 \text{ km s}^{-1}$ are attributable to the $[NII] 6548 \text{ \AA}$ line emission that falls in the wings of the interference filter and that is separated from the $H\alpha$ emission by about 0.5 order of interference. The localization of the high-velocity gas emitting in the range from 200 to 400 km s^{-1} is shown in the central $H\alpha$ image of the PWN (isophotes).

$H\alpha$ lines over the entire $16' \times 16'$ field whose image is given in the paper by Hester and Kulkarni (1989).

The filamentary morphology and the intense $[SII]$ line emission provide strong evidence for the gas emission behind the shock front. It is interesting to measure the velocities of these filaments in the extended remnant outside the core, since, in general, the thin filaments can be localized on the front or rear side of the old shell; i.e., these may be projected rather than be physically associated with the PWN. Besides, the pulsar's velocity with respect to the ambient gas is important in estimating the expected shape of the bow shock produced by the wind

from a fast-moving pulsar. Figure 4 (bottom panel) shows only the brightest outer filaments in a $4' \times 4'$ field for which the background subtraction effect is insignificant (see above). The $H\alpha$ brightness of these filaments exceeds $8.6 \times 10^{-17} \text{ erg s}^{-1}/\square''$. As follows from Fig. 4 (bottom), the velocities of the bright filaments in the outer shell of CTB 80 do not differ significantly from the velocities of the peripheral filaments of the PWN undistorted by the expansion of the latter.

Note, in particular, the filaments that are immediately adjacent to the PWN in the north and the east and that form a kind of a wake at the boundary of the shell pro-

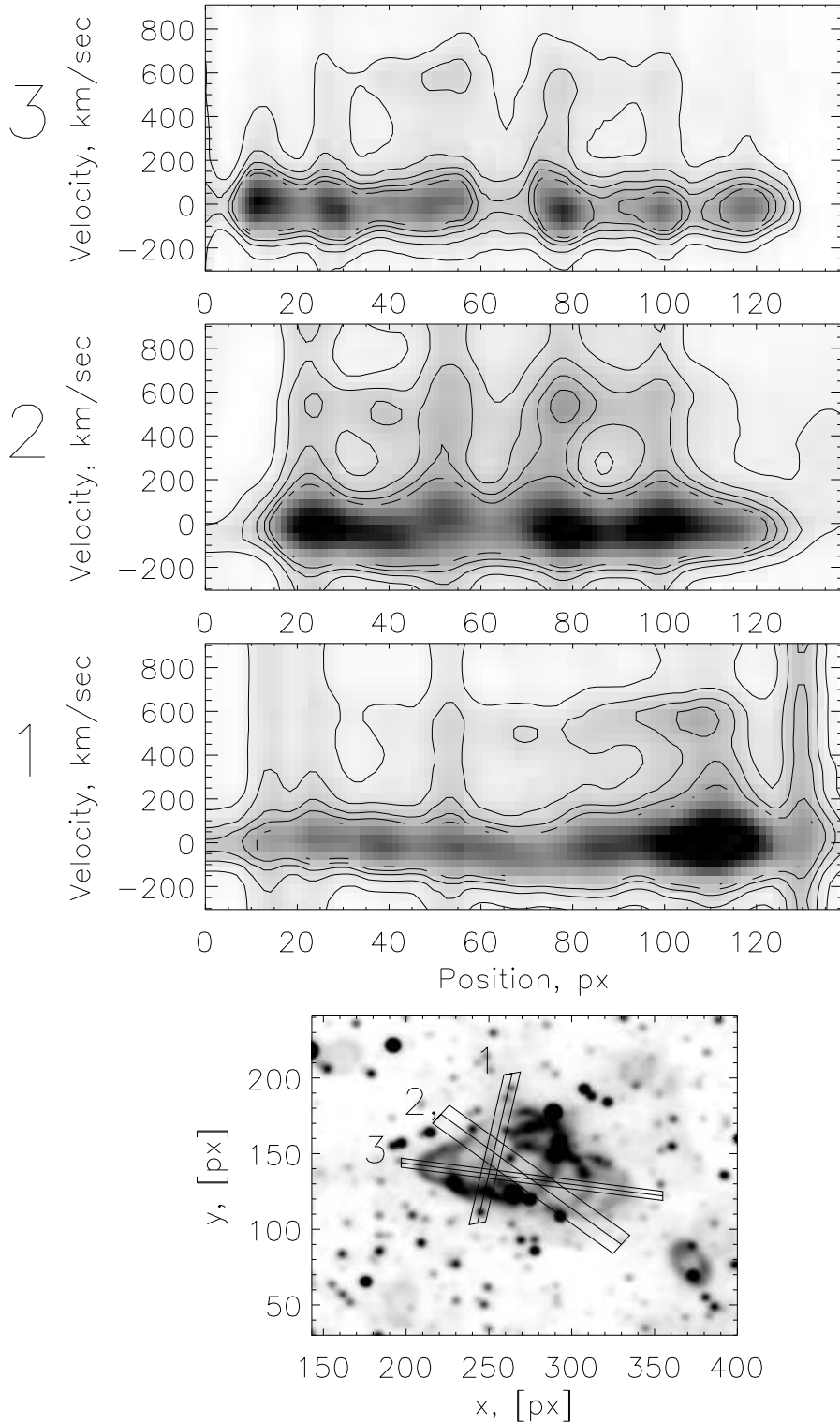


Fig. 3. Position–velocity diagrams constructed from our FPI observations and the localization of the corresponding scans in the PWN image. The emission features at a velocity of about 600 km s^{-1} are attributable to the $[\text{NII}] 6548 \text{ \AA}$ line.

duced by the wind from a moving pulsar. (These filaments are most distinct in the $[\text{SII}]$ lines in Fig. 2b from Hester and Kulkarni 1989). As our measurements indicate, the velocities of these filaments do not differ significantly from those of the bright PWN filaments either.

DISCUSSION

The difficulty of explaining the nature of the PWN in CTB 80 lies in the fact the bow-shock structure (in the $[\text{OIII}]$ line, the radio continuum, and the soft X-ray band)

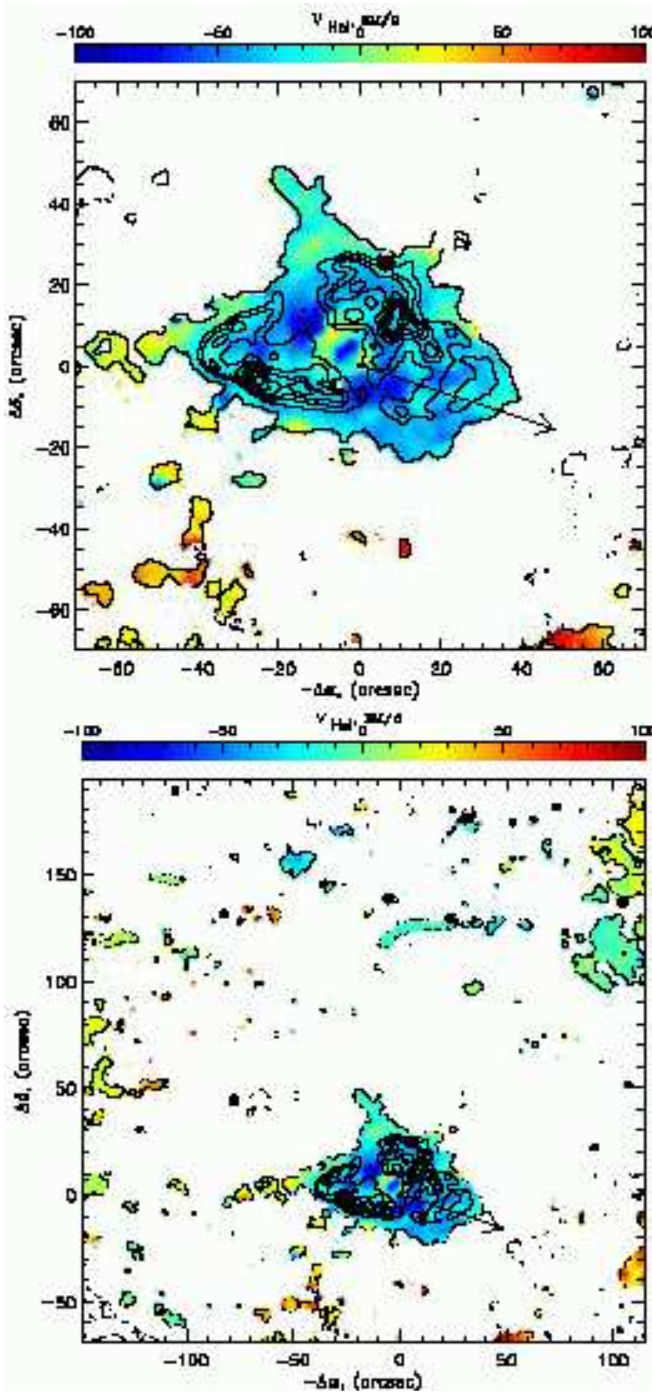


Fig. 4. CTB80 core. *Top panel:* the velocity field of the $H\alpha$ peak superimposed on the PWN image. The arrow indicates the direction of the pulsar’s motion, as measured by Migliazzo *et al.* (2002); *bottom panel:* the same for the entire FOV of about $5' \times 5'$ in size in the image obtained with the 6 m telescope (only the brightest outer filaments are shown).

and the elongated filamentary shell-like structure in the $H\alpha$ line, which is definitely also of an shock origin that, in the opinion of Hester (2003), is associated with the action of the pulsar’s jets, are simultaneously clearly seen around the pulsar. We do not see any manifestations of the inter-

action between two processes: the ejections of relativistic pulsar plasma in two jets and the motion of the pulsar. The elongated PWN structure is not distorted by the pulsar’s motion in any way; the bow shock, in turn, is not distorted by the action of the two plasma jets in any way either. The rough estimates given below indicate that individually both structures can be explained adequately.

Estimates for the Shock Waves Produced by the Pulsar’s Jets

If the pulsar’s power L is constant over time t and is released in a solid angle Ω , blowing a bubble of radius $R = R(t)$ in a homogeneous interstellar medium with a density ρ_0 , then the mass $M \sim \Omega\rho_0 R^3/3$ is swept up from the bubble. Assuming that all of this mass is gathered in a thin layer at radius R and remains in the same solid angle Ω (in fact, it will partially flow around the jet) and equating the pulsar-wind momentum flux L/c to the rate of increase in the momentum of the wind-driven shell,

$$\frac{L}{c} = \frac{d}{dt}(Mv),$$

where $v = dR/dt$, we obtain an acceptable size of the bubble swept up by the wind for a pulsar at rest under reasonable assumptions about the ambient density and the wind asphericity. Assuming that $R \propto t^\alpha$, we have

$$\frac{L}{c} = \frac{\Omega}{3}\rho_0\alpha\frac{d}{dt}\left(\frac{R^4}{t}\right);$$

hence, $\alpha = 1/2$ at $L = \text{const}$, i.e.,

$$R = \left(\frac{6L}{\Omega c\rho_0}\right)^{1/4} t^{1/2} \sim 3 \text{ pc} \times \left(\ell L_{36} \frac{4\pi}{\Omega n_0}\right)^{1/4} t_6^{1/2}, \quad (1)$$

where $\ell = L/L_0$ is the fraction of the power L_0 went into the solid angle Ω and spent on blowing the bubble, n_0 is the particle number density (for hydrogen composition), and t_6 is the time in Myr.

The power of the flux in relativistic particles (including all types of photons) from the pulsar PSR B1951+32 is $L_0 = \dot{E}_{\text{rot}} = 3.7 \times 10^{36} \text{ erg s}^{-1}$ (Kulkarni *et al.* 1988). At $n_0 = 1 \text{ cm}^{-3}$, $L_{36} = 3.7$, and the pulsar’s total age $t_6 = 0.1$, we obtain a bubble size of about 1 pc at $\ell = 1$ even for isotropic radiation ($\Omega = 4\pi$), in agreement with the observed PWN size in the $H\alpha$ line. In fact, only a small fraction ℓ of the pulsar’s power goes into blowing the bubble, but Ω is also much less than 4π (by several hundred times for a linear jet opening angle of several degrees).

We emphasize that this is the minimum upper limit: here, the shock waves are assumed to be radiative. The bubble size will increase if the hot-gas pressure inside the bubble is taken into account (Castelletti *et al.* 2003). Two cases are possible: the radius for radiative shock waves is larger than our estimate, but smaller than that for adiabatic shock waves (McKee and Ostriker 1977; Blinnikov *et al.* 1982).

If we took into account the hot-gas pressure inside the bubble and for adiabatic shock waves, we would obtain the maximum estimate at $\Omega = 4\pi$ (Avedisova 1971; Weaver *et al.* 1977; Ostriker and McKee 1988):

$$R = 28 \text{ pc} \times n_0^{-1/5} L_{36}^{1/5} t_6^{3/5}. \quad (2)$$

Hence, R could be even an order of magnitude larger than that from (1).

Let us make several remarks suggesting that these rough estimates are uncertain. On the one hand, the Balmer line emission in PWNs is evidence of nonradiative shock waves in a partially neutral medium (Chevalier and Raymond 1980); it is produced by electron impact excitation or ion charge exchange. In this case, neutral hydrogen can penetrate into the hot gas and impart odd shapes to the shock waves (Bucciantini and Bandiera 2001; Bucciantini 2002; D’Amico *et al.* 2003)

On the other hand, formula (2) was derived for a hot wind with a normal (Pascal) pressure. Since the flow of magnetized particles or photons in a pulsar wind is directed only along the radius, a simple formula of form (1) the derivation of which assumes no pressure isotropy holds good, while formula (2) overestimates the result. Many problems associated with the composition of this wind have not yet been solved (the so-called sigma paradox — the transition from the fraction of the electromagnetic pressure expressed in terms of the Poynting vector to the kinetic pressure of the particle flux cannot be reliably calculated (see the review by D’Amico *et al.* 2003)).

A time shorter than the pulsar’s age should be taken as t_6 , since it has flown into the dense layers of the shell of the old SNR relatively recently. Castelletti *et al.* (2003) took $t = 18\,200\text{yr}$ as the PWN age at an ambient density of $n_0 = 0.5 \text{ cm}^{-3}$. According to Mavromatakis *et al.* (2001), the relative line intensities in the spectrum of the filaments of the extended CTB 80 shell are typical of the gas radiation behind the front of a shock propagating at a velocity of $85\text{--}120 \text{ km s}^{-1}$ in a medium with an initial density of about $2\text{--}5 \text{ cm}^{-3}$. This density is equal to the mean density in the HI shell estimated by Koo *et al.* (1990).

However, the dependence of R on all parameters, including the density and the age, is weak; i.e., clearly, a small fraction ℓ of the total power that goes into blowing the bubble will suffice. (We also see the pulsar’s emission; i.e., clearly, the fraction of the captured power, ℓ , is appreciably smaller than unity.)

Thus, the sizes of the bubbles swept up by the pulsar-wind jets can easily be made close to the observed values even if the density is much higher and the fraction ℓ of the pulsar’s power that goes into the jet is small.

An Estimate for the Location of the Bow Shock

The pulsar’s motion in the plane of the sky with a velocity of $v_0 = 240 \text{ km s}^{-1}$ (Migliazzo *et al.* 2002) for an *isotropic* wind must give rise to a bow shock, which is observed in several pulsars (see the review by D’Amico *et al.* 2003).

To estimate the shock shape, we can use the solutions by Lipunov and Prokhorov (1984) and Wilkin (1996). The latter author obtained an analytical solution for a normal (nonrelativistic) stellar wind with radiative shock waves:

$$R(\theta) = d_0 \csc [3(1 - \theta \cot \theta)]^{1/2}, \quad (3)$$

where d_0 is the distance from the pulsar to the head point at contact discontinuity. This solution describes well the classical numerical results by Baranov *et al.* (1971) and van der Swaluw *et al.* (2003), see Fig.8 in the latter. An approximate solution for adiabatic shock waves was given by Chen *et al.* (1996). The criticism of the applicability of such solutions to known PWNs (see Bucciantini and Bandiera 2001) is based on the fact that these do not include the effects of charge exchange and neutral hydrogen penetration behind the shock mentioned above. However, the PWN in CTB 80 is unique in that the bow shock is observed not only in Balmer lines, but also, most clearly, in [OIII] lines and in the X-ray and radio bands, i.e., in a hot, ionized plasma. Therefore, simple analytical solutions may well be valid in this case.

We obtain the following estimate from the balance between the momentum fluxes $\ell_1 L/c$ and $4\pi d_0^2 \rho_o v_0^2$:

$$d_0 = \left(\frac{\ell_1 L}{4\pi c \rho_o v_0^2} \right)^{1/2}. \quad (4)$$

Hence, we find for $v_0 = 240 \text{ km s}^{-1}$, $\rho_o = 2 \times 10^{-24} \text{ g cm}^{-3}$ ($n_0 = 1 \text{ cm}^{-3}$), and $\ell_1 = 1$ that $d_0 \approx 0.044 \text{ pc}$. This value is comparable to the observed distance from the pulsar to the [OIII] filaments that determine the position of the head point at the shock front, $d_{\text{obs}} \sim 6'' \approx 0.057 \text{ pc}$.

The theoretical value of d_0 will be close to d_{obs} if we take into account the fact that $v_0 = 170 \text{ km s}^{-1}$ should be substituted for $v_0 = 240 \text{ km s}^{-1}$, since the pulsar moves in the matter of a remnant expanding with a velocity of 72 km s^{-1} . In this case, $d_0 \approx 0.043 \text{ pc}$.

In Fig. 5 (top panel), the solution by Wilkin (1996) is superimposed on the PWN image in the [OIII] line and in the radio continuum. The distance from the head point at the front to the pulsar is assumed to be $d_0 \approx 0.043 \text{ pc}$, and the axis of the surface with a position angle of 235° does not coincide with the pulsar’s velocity direction in the plane of the sky. An azimuthal asymmetry in the projection of the theoretical surface relative to the observed shape of the central shell remains noticeable at a position angle of $P = 252^\circ$ according to the measurements by Migliazzo *et al.* (2002).

The fact that the shape of the bow shock observed in the [OIII] line is appreciably “broader” than the gas-dynamical solutions by Wilkin (1996) may suggest that the pulsar moves at a significant angle to the plane of the sky. Allowing for the possible inclination of the pulsar’s velocity vector to the plane of the sky yields better agreement of the theory with the observed morphology of the central shell. By varying the pulsar’s velocity vector, we found the best agreement with the observations for a bow shock whose axis is inclined at an angle of 60° to the plane

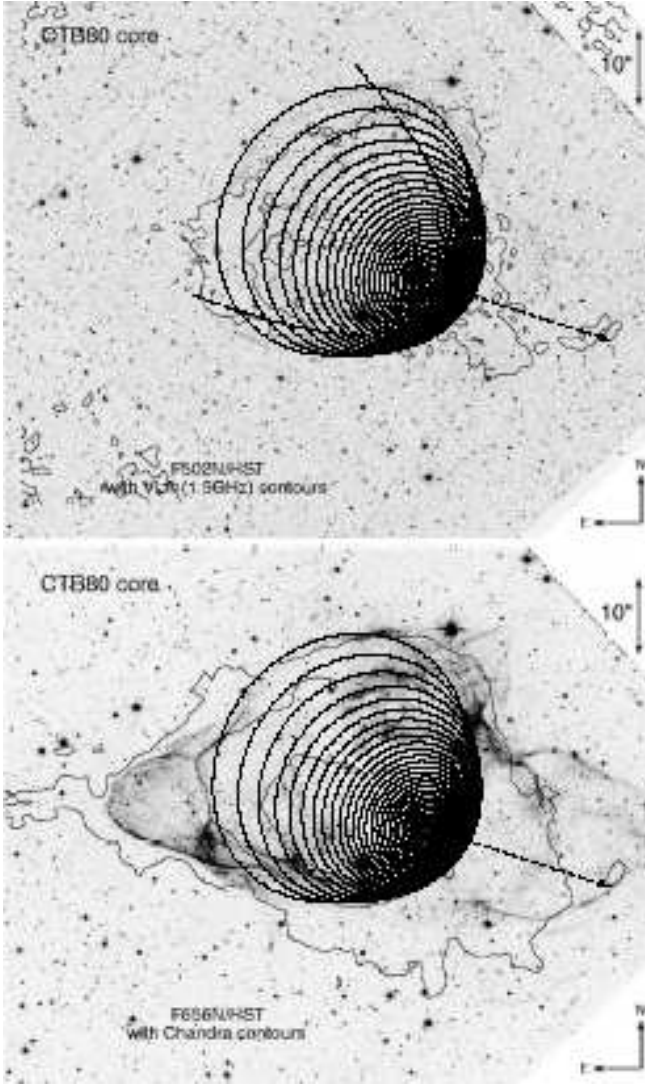


Fig. 5. *Top panel:* PWN in the [OIII] line and in the radio continuum (isophotes): the bow shock corresponding to solution (3) for the pulsar’s motion in the plane of the sky with a position angle of 235° (dashed line) and the bow shock inclined at an angle of 60° to the plane of the sky (θ isolines). *Bottom panel:* The same bow shock inclined at an angle of 60° chosen by the best agreement with the [OIII] line image superimposed onto the $H\alpha$ and X-ray image (isophotes) of the PWN. The arrow indicates the pulsar’s motion over a period of 1000 yr, as measured by Migliazzo et al. (2002).

of the sky. Figure 5 (top panel) shows this solution for the bow shock chosen by the best agreement with the shape of the central shell observed in the [OIII] line and in the radio continuum. As we see, the shape of the projection of the theoretical surface defined by relation (3) can be completely reconciled with the observed PWN morphology. In this case, the position angle of the pulsar’s velocity vector in the plane of the sky is $P = 235^\circ$; i.e., it is close to the direction of the symmetry axis in the velocity field of the

main $H\alpha$ line component found above. $P = 235^\circ$ matches the value obtained by Strom (1987).

We emphasize that, if the pulsar’s velocity vector is inclined at an angle of 60° , its space velocity is twice as high as its velocity measured in the plane of the sky; i.e., it reaches 500 km s^{-1} (this value agrees with the mean value in the velocity distribution of pulsars; see Arzoumanian et al. 2002.) Since the distance d_0 at a higher velocity is a factor of $\sqrt{2}$ smaller, for close agreement with the observations, we must take a slightly lower gas density in front of the bow shock.

Our kinematic studies are also consistent with the suggested model. Since the thickness of the postshock emitting gas, which is determined by the apparent thickness of the bright peripheral PWN filaments, is an order of magnitude smaller than the distance the pulsar traverses in 1000 yr, (see Fig. 1), we conclude that the radiative cooling time of the postshock gas is short, about 100 yr. In this time, an element of gas is not only compressed, but also acquires a velocity that corresponds to the pulsar’s motion. Without detailed calculations, it is hard to tell at which velocity the gas emission is at a maximum; one may only expect the observed velocity to be a significant fraction of the pulsar’s velocity.

Gas motions with such velocities in the PWN have been detected in our work for the first time (see above). These velocities refer to the weak emission features in the $H\alpha$ line; they are observed both in the central region around the pulsar, and near the bright filaments at the PWN boundary (see Fig. 2). The line-of-sight velocities of the bright filaments are within the $\pm 200 \text{ km s}^{-1}$ range. This is an ordinary (for SNRs) situation related to the fact that the bright filaments usually represent the front surfaces seen edge-on.

Unfortunately, since the velocity measurement range in our FPI observations is limited, at present, we cannot unambiguously determine whether the pulsar is moving toward or away from us. The existence of high positive velocities argues for the motion away from us, but as yet we have no information about the possible negative velocities without further FPI observations. The derived velocity distribution of the line peak could clarify the picture, but here we are restricted by the fact that the density distribution in the closest neighborhood of the shell corresponding to the bow shock is unknown. In particular, the asymmetric expansion of the central shell (according to Whitehead et al. (1989), the motion of the approaching side at a velocity of about -200 km s^{-1} is most clearly observed in it) could be attributable to the higher brightness of this side due to a nonuniform ambient gas density.

In Fig. 5 (bottom panel), the same theoretical surface of the bow shock that is inclined at an angle of 60° to the plane of the sky and that agrees best with the PWN emission in the [OIII] line is superimposed on the $H\alpha$ image with X-ray isophotes. The two shell-like $H\alpha$ structures in the west and the east are far outside the bow shock. These structures, which form the elongated PWN shape, were explained by the action of the pulsar’s jets (Hester 2000).

It should be noted that, if the pulsar’s jets are directed at an angle to its space velocity (e.g., lie in the plane of the sky), then the contradiction with the absence of an apparent influence of the jets on the shock front in its brightest parts mentioned at the beginning of the section is removed.

Of course, the representation of the shock as an infinitely thin layer with shape (3) is oversimplified. More detailed solutions should be used, and the structure of two shocks with a contact discontinuity between them should be taken into account (Baranov *et al.* 1976), since there is a hint at such a structure in the observations. In particular, Moon *et al.* (2004) associate the structure observed in X rays with a backward shock wave in the pulsar wind and in the H α line with a bow shock in the ambient medium.

Note also that, in fact, ℓ_1 in formula (4) may be the fraction of the pulsar’s emission absorbed by an ionized plasma, while ℓ in formula (1) for the jet may be the fraction of the emission absorbed by neutral hydrogen. For example, hard ultraviolet emission must be absorbed completely by neutral hydrogen and only partially by ionized plasma. Another possible process, the proton-beam charge exchange in a neutral gas, cannot take place in an ionized medium. Thus, different components of the pulsar’s flux can manifest themselves differently in different components of the ambient medium.

A different interpretation of the elongated PWN shape in the H α line is also possible. The system of thin filaments mentioned in the Section “Results of Observations”, which characterizes the optical emission from the extended remnant outside the PWN, is most likely the layered structure of the old CTB 80 shell (Hester and Kulkarni 1989). Our velocity measurements for the brightest filaments suggest that these are not projected, but are physically associated with the PWN.

The thickness of the layers (typically, ~ 10 – $20''$ or 0.1–0.2 pc) and the separation between them (about $2'$ – $2.5'$ or 1–1.5 pc) at the pulsar’s velocity of 240 km s^{-1} in the plane of the sky yield a time of about 5000 yr between the passages of neighboring layers and a passage time of a dense layer of 400–800 yr.

The pulsar’s motion through such a layered medium can produce the observed elongated multishell structure of the core as a result of the pulsar-wind breakthrough from a dense layer into a tenuous medium between the layers. The breakthrough of the nonrelativistic wind of Wolf–Rayet stars from a dense cloud into a tenuous intercloud gas leads precisely to this effect (see, e.g., Dopita and Lozinskaya 1990).

Localization of the Pulsar in the Extended Remnant CTB 80

If the space velocity of the pulsar actually reaches 500 km s^{-1} , then, in general, it traverses a distance of 50 pc in a time of 10^5 yr and could go beyond the symmetric infrared and HI shells about 40 pc in size, accord-

ing to the previous interpretation, determined the total volume of the old remnant CTB 80. However, the deep images taken in the H α + [NII], [SII], [OII], [OIII] lines by Mavromatakis *et al.* (2001) revealed large-scale filamentary and diffuse structures in the nearby $2^\circ \times 2^\circ$ region. These optical filaments in the north and the northwest closely correlate with the radio images of the remnant (Castelletti *et al.* 2003) and with the boundary of the infrared shell, but go far beyond the infrared and HI shells in the south and the east. (Here, we disregard the extended filaments in the east associated not with CTB 80, but with the remnant of a different supernova (Mavromatakis and Strom 2002).) The relative line intensities in the spectrum of these large-scale filaments are typical of the radiative cooling of the gas behind the front of a shock propagating at a velocity of 85 – 120 km s^{-1} in a medium with an initial density of about 2 – 5 cm^{-3} (Mavromatakis *et al.* 2001). Such a density agrees with the mean density in the HI shell estimated by Koo *et al.* (1990) from 21-cm line observations. This argues for the association of the large-scale filaments with the SNR CTB 80.

Therefore, a more complex spatial structure composed of two hemispheres with different sizes should probably be considered as the SNR CTB 80. One hemisphere, which is determined by the northeastern radio ridge and the infrared and HI shells, is the result of the interaction of the shock triggered by a supernova explosion with a dense medium. The second part of the shell has an aspherical shape and is determined by the southwestern ridge and the [OIII] filaments denoted by III and IV as well as by the system of bright filaments to the east of IV (see Fig. 2 from Mavromatakis *et al.* 2001). This part of the shell was most likely formed by the shock in a medium with a much lower density.

Figure 6 shows approximate boundaries of the two parts of the shell in projection onto the plane of the sky in this model.

Note that ROSAT observations revealed a conical $\sim 1^\circ$ region of thermal X-ray emission southeast of the pulsar far beyond the infrared shell (Safi-Harb *et al.* 1995). The central region of the second part of the shell mentioned above could, in principle, be responsible for this emission. However, the SNR CTB 80 is observed along the Cygnus spiral arm and is immediately adjacent to the giant Superbubble produced by intense stellar wind from the Cyg OB2 cluster (Lozinskaya *et al.* 2002, and references therein). Therefore, in general, the thermal X-ray emission in the extended conical region could be the background emission, i.e., it could belong not to CTB 80, but to the Superbubble.

In the proposed scheme, the morphology of the SNR in the plane of the sky suggests that the major axis of this structure composed of two hemispheres with different sizes is oriented at a large angle to the plane of the sky. Therefore, at a possible space velocity of 500 km s^{-1} , the pulsar has not yet gone outside the shell of the extended remnant CTB 80.

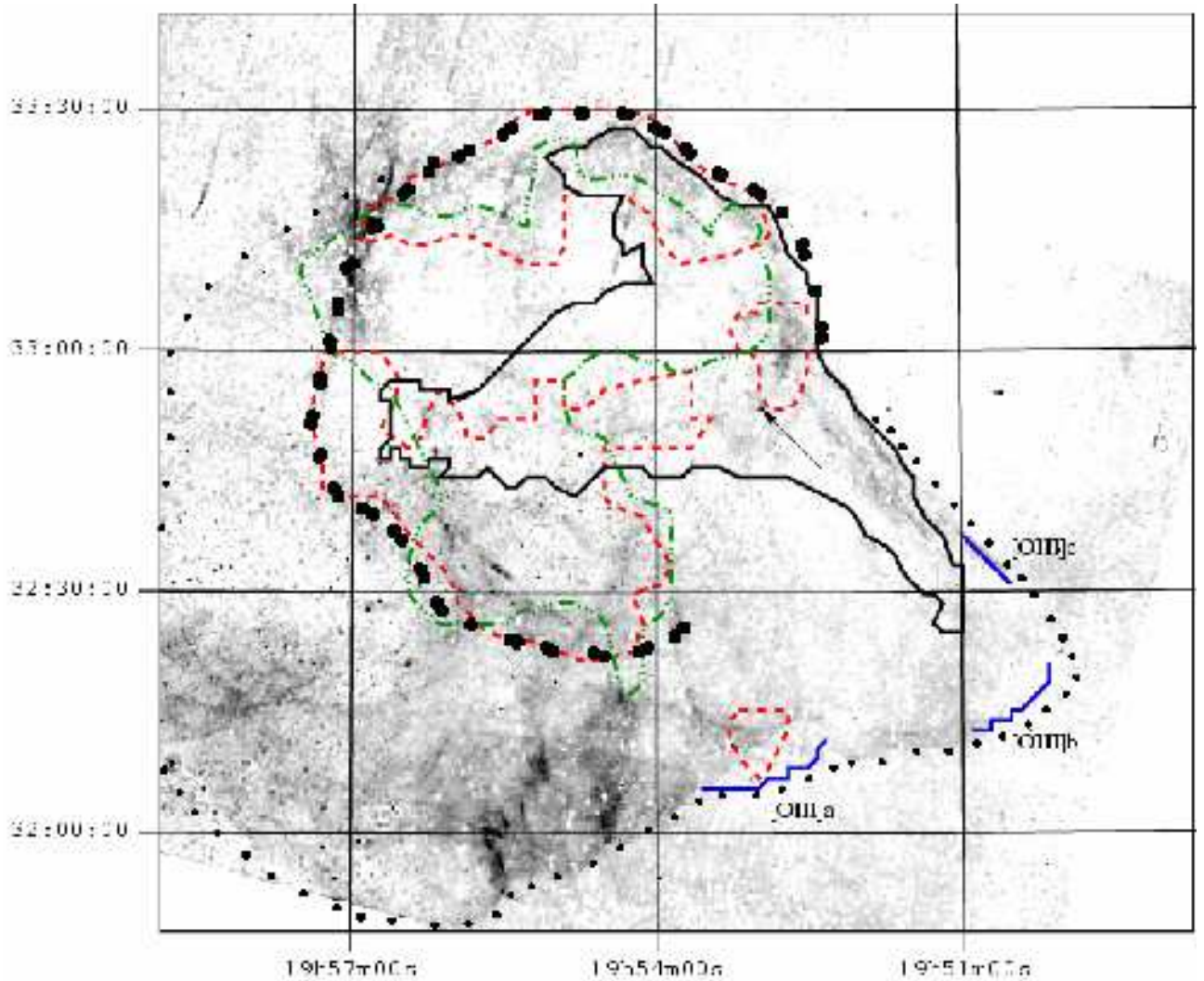


Fig. 6. General scheme of CTB 80 from Mavromatakis *et al.* (2001): the [SII] image of the region, radio ridges (solid line), and the infrared and HI shells (the dashed and dash-dotted lines, respectively). The large and small circles indicate the suggested model for the shell of the old SNR composed of two hemispheres in projection onto the plane of the sky.

CONCLUSIONS

Our kinematic study of the pulsar wind nebula in the old supernova remnant CTB 80 using the FPI of the 6 m SAO telescope has revealed weak high-velocity $H\alpha$ features in the PWN at least up to a velocity of 400–450 km s^{-1} . We confirmed the previously measured expansion of the system of bright filaments with a velocity of 100–200 km s^{-1} . We analyzed the PWN morphology in the $H\alpha$, [SII], and [OIII] lines using the HST archival data. The shape of the bow shock, which is determined by the central horseshoe-shaped shell bright in the [OIII] line and in the radio continuum, was shown to be in best agreement with the theory for a significant (about 60°) inclination of the pulsar’s velocity vector to the plane of the sky. The space velocity of the pulsar is twice as high as its tangential velocity measured by Migliazzo *et al.* (2002); i.e., it reaches 500 km s^{-1} . This pattern of motion is also confirmed by the high radial velocities of the gas in the PWN that we found here. Thus,

PSR B1951+32 is the first pulsar whose possible light-of-sight velocity (of about 400 km s^{-1}) has been estimated from the PWN morphology and kinematics.

The filamentary shell-like structures observed in the $H\alpha$ line in the east and the west outside the bow shock can be explained not only by the action of the pulsar’s jets, but also by the pulsar-wind breakthrough into an inhomogeneous ambient medium.

We considered the general scheme of CTB 80 that includes the most recent optical and radio observational data in which the pulsar’s high space velocity is consistent with its location in the dense shell of the old SNR.

Of course, the proposed scheme of the PWN in CTB 80 must be confirmed additionally. The existence of high velocities in the PWN, the pattern of elongated $H\alpha$ structures (possibly under the influence of the pulsar’s jets or when the wind breaks through from a thin dense layer), and other questions require further observations and de-

tailed hydrodynamic simulations of this interesting object. An analysis of the velocity field for the extended filaments in the entire region can give a kinematic confirmation for the proposed scheme of the old SNR CTB 80.

1. ACKNOWLEDGMENTS

This work was supported by the Russian Foundation for Basic Research (project nos. 02-02-16500, 03-02-17423, 04-02-16042) and the Federal Science and Technology Program (contract no. 40.022.1.1.1103). A.V. Moiseev thanks the Russian Sciences Support Foundation for partial support of this work. We are grateful to Yu.A. Shibano for a kind permission to use the data obtained as part of his observational program on the 6m BTA telescope, B.M. Gaensler for providing the VLA radio data and I.V. Karamyan, V.Yu. Avdeev, and O.V. Egorov for help. This work is based on the observational data obtained with the 6m SAO telescope financed by the Ministry of Science of Russia (registration no. 01-43) and on the NASA/ESA Hubble Space Telescope data taken from the archive of the Space Telescope Science Institute operated by the Association of Universities for research in astronomy under a NASA contract (NAS 5-26555) and data of the Chandra X-ray Observatory Center, which is operated by the Smithsonian Astrophysical Observatory for and on behalf of the National Aeronautics Space Administration under contract NAS8-03060.

References

- V. L. Afanasiev and A. V. Moiseev, *Pis'ma Astron. Zh.* **31**, 214 (2005), [*Astron. Letters*, 31, 193, (2005)]
- P. E. Angerhofer, R. G. Strom, T. Velusami, *et al.* *Astron. Astrophys.* **94**, 313 (1981).
- P. E. Angerhofer, A. S. Wilson, and J. R. Mould, *Astrophys. J.* **236**, 143 (1980).
- Z. Arzoumanian, D.F. Chernoff, and J.M. Cordes, *Astrophys. J.* **568**, 289 (2002).
- V. S. Avedisova, *Astron. Zh.* **48**, 894 (1971) [*Sov. Astron.* **15**, 708 (1972)].
- V. B. Baranov, K. V. Krasnobaev, and A. G. Kulikovskii, *Dokl. Akad. Nauk SSSR* **194**, 41 (1971) [*Sov. Phys.-Dokl.* **15**, 791 (1971)].
- V. B. Baranov, K. V. Krasnobaev, and M. S. Ruderman, *Astrophys. Space Sci.* **41**, 481 (1976).
- S. I. Blinnikov, V. S. Imshennik, and V. P. Utrobin, *Pis'ma Astron. Zh.* **8**, 671 (1982) [*Sov. Astron. Lett.* **8**, 361 (1982)].
- W. P. Blair, R. A. Fesen, and R. H. Becker, *Astron. J.* **96**, 1011 (1988).
- W. P. Blair, R. P. Kirshner, R. A. Fesen, *et al.*, *Astrophys. J.* **282**, 161 (1984).
- N. Bucciantini, *Astron. Astrophys.* **387**, 1066 (2002).
- N. Bucciantini, *Astron. Astrophys.* **393**, 629 (2002).
- N. Bucciantini and R. Bandiera, *Astron. Astrophys.* **375**, 1032 (2001).
- G. Castelletti, G. Dubner, K. Golap, *et al.*, *Astron. J.* **126**, 2114 (2003).
- Y. Chen, R. Bandiera, and Z. Wang, *Astrophys. J.* **469**, 715 (1996).
- R. A. Chevalier and J. C. Raymond, *Astrophys. J.* **225**, L27 (1980).
- N. D'Amico, R. Bandiera, N. Bucciantini, *et al.*, *Mem. Soc. Astron. Italiana* **74**, 345 (2003).
- M.A. Dopita and T.A. Lozinskaya, *Astrophys. J.* **359**, 419 (1990).
- R. A. Fesen, J. M. Shull, and J. M. Saken, *Nature* **334**, 229 (1988).
- A.S. Fruchter, J.H. Taylor, D.C. Backer, *et al.*, *Nature* **331**, 53 (1988).
- J. J. Hester, *Proc. Conf. "Spin, Magnetism and Cooling of Young Neutron Stars"*, *Kavli Institute of Theoretical Physics, 2000*, <http://online.itp.ucsb.edu/online/neustars.c00/hester/>.
- J. J. Hester, *Bull. Am. Astron. Soc.* **32**, 1542 (2000).
- J. J. Hester and S. R. Kulkarni, *Astrophys. J.* **331**, L121 (1988).
- J. J. Hester and S. R. Kulkarni, *Astrophys. J.* **340**, 362 (1989).
- B.-C. Koo, W.T. Reich, C. Heiles, *et al.*, *Astrophys. J.* **364**, 178 (1990).
- B. C. Koo, M. S. Yun, P. T. P. Ho, *et al.*, *Astrophys. J.* **417**, 196 (1993).
- S. R. Kulkarni, T. C. Clifton, D. C. Backer, *et al.*, *Nature* **331**, 50 (1988).
- V.M. Lipunov and M.E. Prokhorov, *Astrophys. Space Sci.* **98**, 221 (1984).
- T. A. Lozinskaya, V. V. Pravdikova, and A. V. Finogenov, *Pis'ma Astron. Zh.* **28**, 260 (2002) [*Astron. Lett.* **28**, 223 (2002)].
- F. Mantovani, M. Reich, C. J. Salter, *et al.*, *Astron. Astrophys.* **145**, 50 (1985).
- F. Mavromatakis and R. G. Strom, *Astron. Astrophys.* **382**, 291, (2002).
- F. Mavromatakis, J. Ventura, E. V. Paleologou, *et al.*, *Astron. Astrophys.* **371**, 300 (2001).
- C. F. McKee and J. P. Ostriker, *Astrophys. J.* **218**, 148 (1977).
- J. M. Migliazzo, B. M. Gaensler, D. C. Backer, *et al.*, *Astrophys. J.* **567**, L141 (2002).
- A. V. Moiseev, *Bull. Spec. Astrophys. Obs.* **54**, 74 (2002); astro-ph/0211104.
- D.-S. Moon, J.-J. Lee, S. S. Eikenberry, *et al.*, *Astrophys. J.* **610**, L33 (2004).
- J. P. Ostriker and C. F. McKee, *Rev. Mod. Phys.* **60**, 1 (1988).
- S. Safi-Harb, H. Ogelman, and J. P. Finley, *Astrophys. J.* **439**, 722 (1995).
- R. G. Strom, *Astrophys. J.* **319**, L103 (1987).
- R. G. Strom, P. E. Angerhofer, and J. R. Dickel, *Astron. Astrophys.* **139**, 43 (1984).
- R. G. Strom and W. P. Blair, *Astron. Astrophys.* **149**, 259 (1985).
- R. G. Strom and B. W. Stappers, *Proc. Conf. "Pulsar Astronomy"* (2000).
- E. van der Swaluw, A. Achterberg, Y. A. Gallant, T. P. Downes, R. Keppens, *Astron. Astrophys.* **397**, 913 (2003).
- T. Velusami and M. R. Kundu, *Astron. Astrophys.* **32**, 375 (1974).
- T. Velusami, M. R. Kundu, and R. H. Becker, *Astron. Astrophys.* **51**, 21 (1976).
- R. Weaver, R. McCray, J. Castor, *et al.*, *Astrophys. J.* **218**, 377 (1977).
- M. J. Whitehead, J. Meaburn, and C. A. Claiton, *Mon. Not. R. Astron. Soc.* **237**, 1109 (1989).
- F.P. Wilkin, *Astrophys. J.* **459**, L3 (1996).